Altimetric Analysis of the Sea-Surface GPS-Reflected Signals

Antonio Rius, Estel Cardellach, and Manuel Martín-Neira, *Senior Member, IEEE*

***Abstract*—We describe the development and implementation of a method for extracting altimetric information using the Passive Reflectometry and Interferometry System (PARIS), i.e., from GPS signals after their reflection off the sea surface. We have formalized one idea laid out in the description of a bistatic system for ocean altimetry using the GPS signal, by Hajj and Zuffada (Jet Propulsion Laboratory), and have extended it to real situations encountered in PARIS aircraft experiments. Second, we have developed the corresponding algorithms to produce real-time altimetric observables to be used in dedicated digital signal processors. Finally, we have applied this method to estimate sea-surface height from one flight experiment in the North Sea off the coast of Norway.**

***Index Terms*—GPS, microwave ocean altimetry, microwave ocean scatterometry, sea-surface reflections.**

I. Introduction

VERY LONG Baseline Interferometry (VLBI), Global Navigation Satellite Systems (GNSSs), and radar altimetry (RA) are based on the measurement of ranges between phase centers of microwave antennas. These measurements are extracted from the cross-correlation functions, or waveforms, between recorded signals with suitable replicas. These measurements are processed to provide time–space coordinates and other parameters of geophysical interest, together with their associated uncertainties, to different points on the Earth surface. The International VLBI Service [1] and the International GNSS Service [2] have the mission to provide data and products based on VLBI and GNSS observations which are used in many Earth Science applications. Dedicated RA instruments have been placed on space platforms and provide data and products used to measure sea-surface properties like sea level or its roughness. Reference [3] provides a good background on RA and its applications.

A different technique based on VLBI, GPS, and RA concepts, termed as Passive Reflectometry and Interferometry System (PARIS), or GNSS Reflectometry (GNSS-R), was proposed in 1993 [4] to provide additional measurements of the sea surface to increase the temporal and spatial coverages of RA measurements. Conceptually, PARIS is a bistatic radar altimeter where the transmitters are GNSS satellites.

In all the cases, the measured ranges are built with different components: geometric delays due to the relative position of the transmitter and the receiver, offsets between the transmitter and receiver clock readings, ionospheric delays induced by the electronic content of the ionosphere, tropospheric delay produced by the refractivity of the troposphere, multipath caused by scattering objects in the vicinity of the receiving antenna, delays inside the transmitter and the receiver, and noise. Any of these components could be considered as signals or as noise, depending on the application and its variability. The effective separation between the different components is based on the assumption that the collected data during an observing period show different signatures for the different effects. Different strategies could be devised to obtain the delay components with sufficient accuracy and precision in different scenarios. Accurate instrumentation and calibration techniques will contribute to this separation, at expenses of the cost. Removing the noise effects by the differentiation of observables is another possibility. Reference [5] provides general discussions on these issues.

The accepted practices in metrology [6] classify the uncertainties into two categories: AQ8

1) type-A uncertainties: those which are evaluated by statistical methods applied to the observables (i.e., least squares fits, root mean square (rms), standard deviations, covariances, etc.);
2) type-B uncertainties: those which are evaluated by using additional relevant information (i.e., data provided in calibration reports, model specifications, etc.).

Those practices are relevant in the emerging GNSS-R field, where different scientific and technological disciplines converge, and a reliable uncertainty budget should be established. See, for instance, the different usage of the term *accuracy* in [7] and [8].

A particular uncertainty could be considered as type A or B, depending on the technique used. For example, the tropospheric delay could be considered type A in VLBI or GNSS for a fixed station during a long observing session but is type B in RA. Because RA is a nadir-looking instrument, it presents more uncertainties of type B than VLBI or GPS instruments, which allow a wider angular diversity. Potentially, GNSS-R could observe reflections far from nadir, but then, the interpretation of the observations in terms of geophysical parameter is less reliable because, in such a case, the models have greater uncertainties.

Manuscript received April 16, 2009; revised August 11, 2009. This paper was supported in part by the Spanish Ministry of Science and Innovation AQ1 under Grants ESP2007-30996-E and AYA2008-05906-C02-02 and in part by AQ2 the European Space Agency (ESA) under Grant ECN 20069/06/NL/EL. The work of E. Cardellach was supported by the Ramón y Cajal Program of the AQ3 Spanish Ministry for Education and Science.

A. Rius and E. Cardellach are with the Institut de Ciéncies de l'Espai, AQ4 Consejo Superior de Investigaciones Cientèficas, Institut d'Estudis Espacials AQ5 de Catalunya, 08193 Bellaterra, Spain.

M. Martín-Neira is with the European Space Research and Technology AQ6 Centre, ESA, 2200 AG Noordwijk, The Netherlands (e-mail: rius@ieec.uab.es). AQ7

Digital Object Identifier 10.1109/TGRS.2009.2036721

The conservative approach is to reject such observations, as Cox and Munk [9] made in their classical measurements of the Sun glistening on the sea surface, when they limited their measurements of the roughness of the sea surface to those gathered when the sun elevation was above 55°.

Schematically, an RA [3] extracts two types of measurements from the waveforms: altimeter ranges (to measure the mean sea level) and parameters describing the sea-surface state. It is assumed in this case that the type-A uncertainties are those produced by the random nature of the recorded signals and the variations of the mean sea level and the sea roughness. The rest are considered as type B. This consideration is forced in this case because the altimeter ranges are completely correlated with the mean sea level, tropospheric delay, instrumental delays, and the radial component of the RA orbit. A similar approach should be taken when considering the use of GNSS-R as an altimeter.

All altimeter data must be postprocessed to produce accurate surface elevation measurements. This postprocessing is called "retracking" and is required because the leading edge of the return waveform deviates from the one produced by reflection off a perfectly smooth surface, causing an error in the telemetered range measurement. There are many different methods described in the literature that are available for retracking altimeter data, mostly based on fitting of a theoretical or empirical model to the data (e.g., [10] and [11]). The Zavorotny and Voronovich [12] model, which might consider geometric, instrumental, and sea-state effects, has been widely used for retracking the GNSS-R waveforms (e.g., [13] and [14]). It either requires *a posteriori* knowledge of the sea-surface state to correct the altimetric range or the model itself is used to invert both altimetric and scatterometric components from the data. The disadvantages of the latter approach are twofold: computing time and dependence on the model. In the following sections, we will provide a procedure to "retrack" the GNSS-R waveforms formally independently of the model and sea-state information, as well as computationally efficient. This technique will separate the altimetric components from the scatterometric components of the range with no need of fitting a model. We will finally apply such a procedure to analyze the data gathered during an aircraft experiment.

II. GNSS-R: Altimetric and Scatterometric Observables

A GNSS-R receiver collects, in addition to the direct signals, the GNSS signals after their reflections from the Earth surface. Its main product is the relative delay between the reflected and direct signals. To that end, the receiver produces the *waveforms*, i.e., the cross-correlation of the incoming signals with a well-known replica of them. The shape of the reflected waveform is the result of adding incoherently the contribution of the different points of the surface, and its shape can be remarkably different by comparison with the one corresponding to the direct signal, as shown in Fig. 1. The shape of the direct waveform is a triangle in amplitude (squared triangle in power). The half width of the triangle corresponds to the time length of the modulation *chip*. The time corresponding to the peak

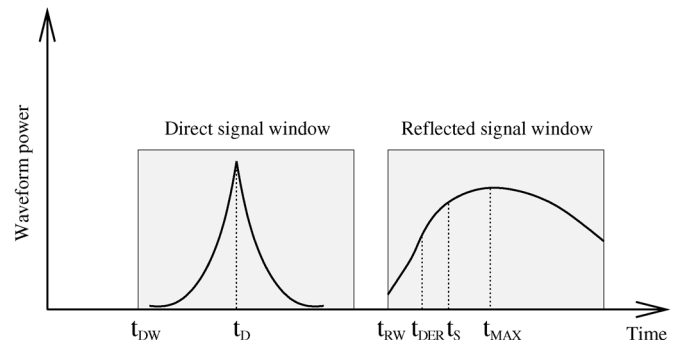

Fig. 1. Direct and reflected waveforms. The cross-correlation is computed in two time windows. The direct window follows the peak of the direct signal using a delay lock loop, and the reflected window position lags the direct signal with a delay computed with *a priori* information based on the real-time navigation information. AQ9

of the direct waveform is taken as the apparent arrival time of the direct signal t_D. In the reflected signal, we will distinguish the time t_{DER} corresponding to the maximum of the derivative of the waveform and the time of the maximum waveform amplitude t_{MAX}. As it will be justified in the next section, the delay corresponding to the maximum of the waveform derivative is a biased estimator of the *specular* delay t_S. In the case of a reflection in a smooth surface, the reflected waveform is also a triangle, and $t_S = t_{\mathrm{DER}} = t_{\mathrm{MAX}}$. The following discussion assumes that $t_S - t_{\mathrm{MAX}}$ is significantly larger than the waveform sampling interval, which is a condition fulfilled when the surface is sufficiently rough.

From these quantities, we define the observed specular delay

$$\Delta\tau_{\mathrm{spec}}^{\mathrm{obs}} \equiv t_{\mathrm{DER}} - t_D \tag{1}$$

and the observed *scatterometric* delay

$$\Delta\tau_{\mathrm{scatt}}^{\mathrm{obs}} \equiv t_{\mathrm{MAX}} - t_{\mathrm{DER}} \tag{2}$$

which contain information related with the position and the sea state, respectively.

The observed specular delay $\Delta\tau_{\mathrm{spec}}^{\mathrm{obs}}$ is obtained using

$$\Delta\tau_{\mathrm{spec}}^{\mathrm{obs}} \equiv (t_{\mathrm{DER}} - t_{\mathrm{RW}}) + (t_{\mathrm{RW}} - t_{\mathrm{DW}}) - (t_D - t_{\mathrm{DW}}) \tag{3}$$

where t_{DW} is the delay corresponding to the origin of the direct window, as measured by the navigation receiver, and t_{RW} is the corresponding value computed by the receiver for the origin of the reflection window.

III. Derivative of the Waveforms: Information Content

Reference [15] presents a theoretical description of a bistatic system for ocean altimetry using a GPS signal. It provides an intuitive framework for the discussion of the capabilities of the PARIS concept from the space. We have taken that paper as a conceptual departure point. Those authors indicate that the delay corresponding to the specular reflection could be obtained by looking for the inflection point of the waveform with positive slope. They support this claim after considering the case of a

waveform built as the limit of an infinite incoherent sum of equal triangles shifted in delay. A search in the open literature has shown that these ideas have not been developed further by the involved community.

Now, we explore some properties of the derivative of the waveforms modeled using the radar equation, as formulated in [12]

$$w(\tau) = T_i^2 \cdot \iint \frac{G \cdot S \cdot \Lambda^2\left[\tau - (R_0 + R)/c\right]}{4\pi R_0^2 R^2} \cdot \sigma_0 \cdot \mathrm{d}^2\rho \tag{4}$$

where T_i is the coherent integration time, ρ is the integration variable, $G = G(\rho)$ is the power gain of the receiving antenna, $S(f(\rho))$ is the sinc-exponential function to account for different frequency f Doppler effects onto different ρ positions, and the triangle function Λ is defined as

$$\Lambda(\tau) = \begin{cases} 1 - |\tau|/\tau_c, & \text{if } |\tau| < \tau_c \\ 0, & \text{otherwise} \end{cases} \tag{5}$$

where τ_c is the chip length, the quantity $\sigma_0(\rho)$ is the normalized bistatic radar cross section of the sea surface, and R_0 and R are the distances from the transmitter and the receiver to point ρ. For the rest of this derivation (Section III), τ is expressed in units of τ_c, whereas the rest of this paper will give the delay in units of length (in meters).

Equation (4) can be written [16] as the convolution product

$$w(\tau) = p(\tau) * \Lambda^2(\tau) \tag{6}$$

where the power per unit delay $p(\tau)$ represents the contribution to the waveform of the points with a delay τ.

If the sea surface was a smooth surface, the shape of the reflected waveform $w(\tau)$ would be the same as the direct waveform but shifted by a delay corresponding to the difference between the delays of the reflected and direct signals. When the surface is not smooth, off-specular (or scattered) reflections are generated, and the reflected power $p(\tau)$ spreads for longer times, starting at the specular delay. Setting the specular delay as $\tau_{\mathrm{spec}} = 0$, it reads

$$\begin{aligned} p(\tau) &= 0, \qquad \tau < 0 \\ &> 0, \qquad \tau \geq 0 \end{aligned} \tag{7}$$

and its derivative could be expressed in these two alternative forms [17]

$$\begin{aligned} w'(\tau) &= p'(\tau) * \Lambda^2(\tau) \\ &= p(\tau) * \Lambda^{2'}(\tau). \end{aligned} \tag{8}$$

The derivative of the squared triangle function is (see also Fig. 2)

$$\begin{aligned} \Lambda^{2'}(\tau) = 2\Lambda(\tau)\Lambda'(\tau) &= 2(\tau + 1), \qquad -1 \leq \tau \leq 0 \\ &= 2(\tau - 1), \qquad 0 < \tau \leq 1 \\ &= 0, \qquad |\tau| > 1. \end{aligned}$$

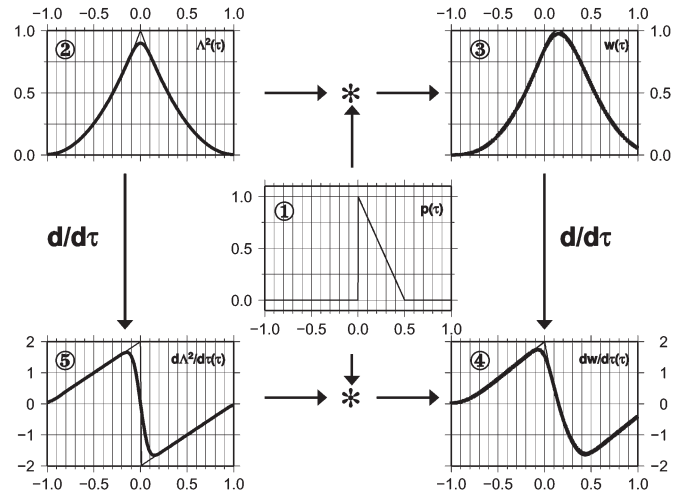

Fig. 2. Panel 1 represents the reflected power as a function of the delay relative to the specular delay, as defined in (7). Panel 2 represents the function $\Lambda^2(\tau)$ defined by (5) as a thin line and its filtered version with a thick line. The following panels use the same convention to represent the unfiltered and filtered versions. The waveform $w(\tau)$ is obtained using (6), and it is represented in Panel 3. Note that both versions are very similar in shape and in the delay corresponding to the maximum power. Panel 4 represents the derivative of the waveform $w'(\tau)$. Now, the position of the derivative depends on the filtered signal. The same results are obtained using the derivative of $\Lambda^2(\tau)$, as indicated in the path which includes Panel 5.

The derivative of the waveform $w(\tau)$(8) will present a peak in the specular point if its second derivative switches sign at that moment, from positive to negative. The second derivative is expressed as

$$w''(\tau) = p(\tau) * \Lambda^{2''}(\tau) \tag{9}$$

$$= \int_{-\infty}^{\infty} p(\tilde{\tau})\Lambda^{2''}(\tau - \tilde{\tau})\,\mathrm{d}\tilde{\tau}. \tag{10}$$

However, $p(\tilde{\tau})$ is defined in $\tilde{\tau} > 0$ (no power earlier than specular ray path)

$$w''(\tau) = \int_{0}^{\infty} p(\tilde{\tau})\Lambda^{2''}(\tau - \tilde{\tau})\,\mathrm{d}\tilde{\tau}. \tag{11}$$

$\Lambda^{2''}(x)$ reads

$$\begin{aligned} \Lambda^{2''}(x) &= 2, \qquad -1 \leq x < 0 \\ &= 2, \qquad 0 < x \leq 1 \\ &= \lim_{\epsilon \to 0} \frac{-4}{2\epsilon}, \qquad -\epsilon < x < \epsilon \\ &= 0, \qquad |x| > 1. \end{aligned}$$

$w''(\tau)$ in (11) is zero when $\tau < -1$. For $\tau \geq -1$, it reads

$$w''(\tau) = \lim_{\epsilon \to 0} \left[\int_{\tau-1}^{\tau-\epsilon} 2p(\tilde{\tau})\,\mathrm{d}\tilde{\tau} + \int_{\tau+\epsilon}^{\tau+1} 2p(\tilde{\tau})\,\mathrm{d}\tilde{\tau} + \int_{\tau-\epsilon}^{\tau+\epsilon} \frac{-4}{2\epsilon} p(\tilde{\tau})\,\mathrm{d}\tilde{\tau} \right]. \tag{12}$$

The last term is

$$\lim_{\epsilon\to 0}\frac{-4}{2\epsilon}\int_{\tau-\epsilon}^{\tau+\epsilon} p(\tilde{\tau})\,\mathrm{d}\tilde{\tau} = \lim_{\epsilon\to 0}\frac{-4}{2\epsilon}2\epsilon p(\tau) = 4p(\tau) \tag{13}$$

and the first and second terms can be expressed as

$$\lim_{\epsilon\to 0} 2\left[\int_{\tau-1}^{\tau-\epsilon} p(\tilde{\tau})\,\mathrm{d}\tilde{\tau} + \int_{\tau+\epsilon}^{\tau+1} p(\tilde{\tau})\,\mathrm{d}\tilde{\tau}\right] = 2\int_{\tau-1}^{\tau+1} p(\tilde{\tau})\,\mathrm{d}\tilde{\tau} \simeq 4\left\langle p(\tau)\right\rangle_{[\tau-1,\tau+1]} \tag{14}$$

with $\langle p(\tau)\rangle_{[\tau-1,\tau+1]}$ being the average value of $p(\tau)$ in the range $[\tau-1,\tau+1]$. Therefore, combining (13) and (14) in (12), the second derivative of the waveform becomes

$$w''(\tau) = 2\int_{\tau-1}^{\tau+1} p(\tilde{\tau})\,\mathrm{d}\tilde{\tau} - 4p(\tau) \simeq 4\left(\left\langle p(\tau)\right\rangle_{[\tau-1,\tau+1]} - p(\tau)\right) \tag{15}$$

i.e., proportional to the difference between the power averaged along two code chip lengths and its instantaneous value.

As stated in (7), there is a positive discontinuity at the delay of the specular point: $p(\tau)$ is zero for $\tau < 0$ and positive for $\tau \geq 0$. If we also assume that $p(\tau)$ is a continuous function monotonically decreasing, then $w''(\tau)$ in (15) will switch from positive to negative sign at the specular point (maximal of a function is greater than the averaged value). Hence

$$t_S = t_{\mathrm{DER}}. \tag{16}$$

Fig. 2 shows graphically the previous discussion. The convolution product of $p(\tau)$, which contains information on the sea state, with $\Lambda^2(\tau)$, which represents the impulse response of the instrument, produces a waveform $w(\tau)$, from which the derivative $w(\tau)'$ is extracted. The thin line corresponds to the ideal case of infinite bandwidth, discussed previously. When we consider a band-limited receiver, the impulse response is filtered, and the results are somewhat different, as indicated by the thick line. Note that, in particular, this filtering introduces a bias in the position of the specular point.

The previous result corresponds to an idealized situation, represented by (6), which is a simplification of (4). A more complete model should include, in addition to the complete radar equation, the consideration of a finite sampling interval of the waveforms in the actual GNSS-R receivers and the presence of different sources of noise: thermal, speckle, and processing noises. With a more complete model, the result equivalent to (16) is

$$t_{\mathrm{DER}} = t_S + \Delta\epsilon_{\mathrm{spec}} \tag{17}$$

where $\Delta\epsilon_{\mathrm{spec}}$ is a correction term which appears when we consider a band-limited version of Λ^2 and a finite sampling rate. This term is zero in the limit case of very large bandwidth and very small sampling rate, in agreement with the analytical discussion; otherwise, it is different from zero. We have estimated this term with a model based on (4) with the actual sampling rate (20 MHz) and bandwidth (10 MHz), and we have found that this term is nearly a bias with a weak dependence on the mean square slope (mss), as indicated in the last column of Table II.

To obtain the result $t_{\mathrm{DER}} = t_S$ with our numerical model, it is required that the separation between t_{MAX} and t_{DER} be large, when measured in the waveform sampling intervals. In the limit case when the surface is flat, we do not have independent information: both delays coincide. If the separation is only a few times the sampling interval of the waveforms, there will be a correlation between both estimates, produced by the processing algorithms used to extract the information. Because the sampling rate is determined by the bandwidth of the signal and the instrument, better results are expected by using instruments and signals with wider bandwidth and higher sampling rates.

IV. Specular and Scatterometric Delay Models

The deterministic specular delay model could be formulated as

$$\Delta\tau_{\mathrm{spec}} \equiv \Delta\epsilon_{\mathrm{spec}} + (t_S - t_D) = \Delta\epsilon_{\mathrm{spec}} + \Delta\tau_{\mathrm{geo}} + \Delta\tau_{\mathrm{ion}} + \Delta\tau_{\mathrm{trop}} + \Delta\tau_{\mathrm{ins,spec}} \tag{18}$$

where the term $\Delta\epsilon_{\mathrm{spec}}$ has been introduced in (17), $\Delta\tau_{\mathrm{geo}}$ is the difference between the geometrical distances of the paths followed by the direct and reflected signals between the transmitter and receiver phase centers, $\Delta\tau_{\mathrm{ion}}$ is the difference between the reflected and direct signals due to the ionosphere, $\Delta\tau_{\mathrm{trop}}$ is the difference between the reflected and direct signals due to the troposphere, and $\Delta\tau_{\mathrm{ins,spec}}$ is the specular instrumental delay which accounts for the biases induced by the differences between the instrumental delays experienced by the reflected and direct signals, and the differences in the extraction processes.

The scatterometric delay model is formulated as

$$\Delta\tau_{\mathrm{scatt}} = (t_{\mathrm{MAX}} - t_{\mathrm{DER}}) = \Delta\epsilon_{\mathrm{scatt}} + \Delta\tau_{\mathrm{ins,scatt}} \tag{19}$$

where the term $\Delta\epsilon_{\mathrm{scatt}}$ is the delay induced by the sea state and $\Delta\tau_{\mathrm{ins,scatt}}$ is a possible bias term produced by the different process followed to extract the quantities t_{MAX} and t_{DER}.

Speckle noise is reduced by the incoherent integration of waveforms, and the thermal noise and processing inaccuracies are expected to be uncorrelated between samples. Table I lists the different sources of uncertainties which we have and its classification as type A or B. The uncertainties associated with the waveform model have two parts: the *a priori* value of the sea-surface state, parameterized as mss, which is considered as type B, and its variation Δmss to be estimated, which is considered as type A. This list is similar to the one corresponding to RA, with the addition of two terms, namely, multipath and carrier-smoothed pseudoranges, which are relevant to the instrument used in the experiment to be discussed later. The

TABLE I
GNSS-R UNCERTAINTIES CLASSIFIED AS TYPE A OR/AND B

Term	Source of uncertainties	Type	Comments
$\Delta\epsilon_{spec}$	Waveform model	A/B	See Section VII
$\Delta\tau_{geo}$	Trajectory	B	Quoted by the provider
	Sea level	A	As in RA. See [3]
$\Delta\tau_{trop}$	Wet delay	B	As in RA. See [3]
	Dry delay	B	Accurate model
$\Delta\tau_{ion}$	Ionosphere	B	Cancels
$\Delta\tau_{ins}$	Instrument	B	Cables
	Smoothed pseudorange	B	See [5]
	Multipath	B	See [5]
$\Delta\epsilon_{scatt}$	Waveform model	A/B	See Section VII

multipath is inherent to the use of low-gain antennas. For the direct signal, we have used "carrier-smoothed pseudoranges," which have reduced multipath, but they are affected by the changes in the ionosphere, as discussed in [5].

V. LINEARIZED MODEL

Using the observables extracted from the integrated waveforms $\Delta\tau_{\text{spec}}^{\text{obs}}$ and $\Delta\tau_{\text{scatt}}^{\text{obs}}$ and the corresponding modeled values, we form the prefit residuals $\delta\tau_{\text{spec}}$ and $\delta\tau_{\text{scatt}}$ as

$$\delta\tau_{\text{spec}} = \Delta\tau_{\text{spec}}^{\text{obs}} - \Delta\tau_{\text{spec}}^{\text{mod}} \tag{20}$$

$$\delta\tau_{\text{scatt}} = \Delta\tau_{\text{scatt}}^{\text{obs}} - \Delta\tau_{\text{scatt}}^{\text{mod}}. \tag{21}$$

We assume that our *a priori* information has the following deficiencies:

1) the variation of the geoidal height of the specular point with respect to the *a priori* value: Δh;
2) a correction term to the *a priori* model of the mss: Δmss;
3) two bias terms b_{spec} and b_{scatt}, which include all the unmodeled effects.

These assumptions allow one to parameterize the two prefit residuals as linear functions of four unknowns

$$\delta\tau_{\text{spec}} = \frac{\partial\tau_{\text{spec}}^{\text{mod}}}{\partial h}\cdot\Delta h + \frac{\partial\tau_{\text{spec}}^{\text{mod}}}{\partial mss}\cdot\Delta mss + b_{\text{spec}} \tag{22}$$

$$\delta\tau_{\text{scatt}} = \frac{\partial\tau_{\text{scatt}}^{\text{mod}}}{\partial h}\cdot\Delta h + \frac{\partial\tau_{\text{scatt}}^{\text{mod}}}{\partial mss}\cdot\Delta mss + b_{\text{scatt}}. \tag{23}$$

Observing different GNSS satellites at different epochs, we will have a series of delays $\delta\tau_{\text{spec}}(sat,t)$ and $\delta\tau_{\text{scatt}}(sat,t)$.

As it has been pointed out in the introduction, the selection of observations near nadir is required for ocean altimetry because the models are more accurate. However, in this case, we have $(\partial\tau_{\text{spec}}^{\text{mod}}/\partial h) \approx -2$, nearly constant, and the estimates of Δh will be highly correlated with b_{spec}.

In VLBI or GNSS positioning, the bias uncertainties could be reduced when the receiver is placed in a fixed position for a long period of time, because in such a case, there is an opportunity of processing observations with a wide range of elevations. Even there, it is recommended to have instrumentation with predictable behavior to reduce the uncertainty. Reference Sec. 6.1.3 [5], entitled *Price of an Inexpensive Receiver Clock*, discusses these issues. An alternative to the bias estimation is to use the differences between observations from a single satellite or different satellites. This approach, used successfully in conventional space geodesy, will fail in our case because the requirement of using high-elevation observations will "dilute the precision." As we will show in Section VII, we will analyze a GNSS-R experiment, and we will show the difficulties of applying space geodetic techniques to real experiments.

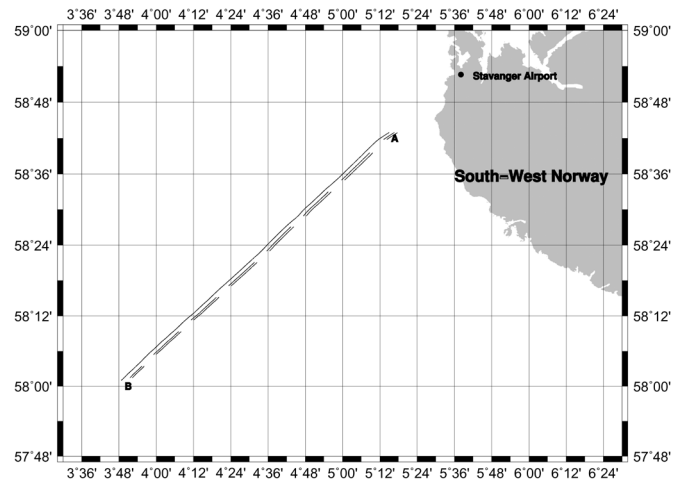

Fig. 3. Distribution of the specular points for the events selected. There are traces for three different satellites: PRN22, PRN19, and PRN3. The aircraft moved from A to B, at roughly 3000-m altitude with an approximate horizontal velocity of 75 m/s, during 1900 s.

VI. EXPERIMENT DESCRIPTION

To test the suitability of the use of the waveform derivative to extract altimetric information, we have analyzed data taken with the GOLD_RTR system described in [18], during an airborne CoSMOS Ocean Salinity Campaign of the European Space Agency (ESA). It took place on April 15, 2006, in front of the southwestern part of the Norwegian coast. The aircraft was moving with an approximate velocity of 75 m/s at roughly 3000-m altitude. General details of the campaign and the scatterometric results have been described in [19].

We have analyzed the data subset obtained while the aircraft followed a straight path and only from GPS satellites with elevation higher than 40°, i.e., GPS satellites with pseudorandom noises (PRNs) 3, 19, and 22. The data set starts at the second of the day 31 780 and for about 1900 s. The satellite with the highest elevation, PRN 19, was observed continuously during this period. The other two were observed only intermittently, alternating 2-min periods of data with 1-min gaps. This was so because the correlators were scheduled to gather data required by the primary experiment, with sea-surface height as a test of opportunity. The altimetry analysis has used only the civil coarse/acquisition (C/A) code of the GPS L1 signals. AQ10 AQ11

The area of the experiment is shown in Fig. 3. The different traces correspond to the specular points for the events selected.

The ellipsoidal altitude of the aircraft as a function of longitude is shown in Fig. 4.

The *a priori* ellipsoidal height of the specular points as a function of longitude is shown in Fig. 4.

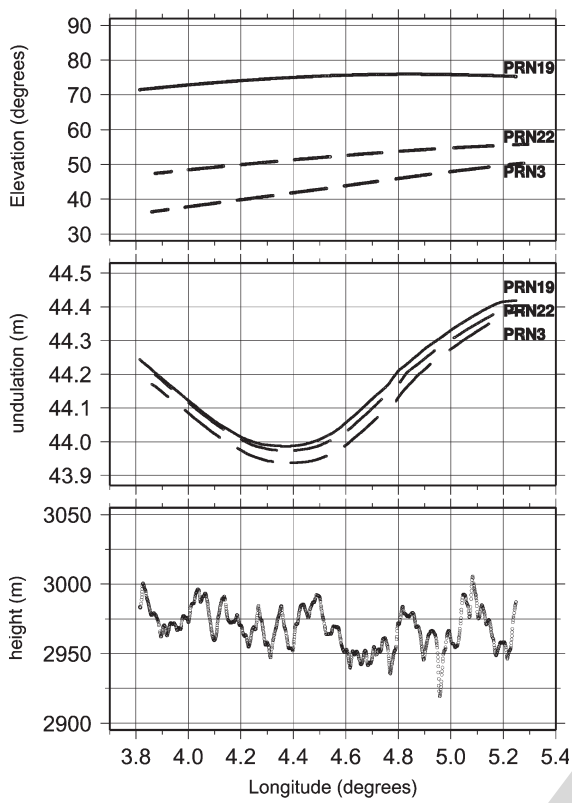

Fig. 4. Upper panel describes the elevation of each satellite as can be seen from the specular point. Note that only satellite PRN19 meets the 55° rule chosen in the Cox and Munk experiment [9]. The middle panel gives the ellipsoidal height of the geoid at the specular point as a function of longitude. The different curves correspond to the different satellites, and the lower panel presents the estimate of the ellipsoidal height of the aircraft during the experiment as a function of longitude. Each point represents 1-s measurement. The variations are on the order of meters, which prevented the accurate estimate of this quantity. Values based on the precise trajectory are computed by the Institut de Geomatica, Barcelona.

To geolocate the integrated waveforms, we also collected the following information:

1) *a priori* geoid grid in the WGS84 reference frame (see [20]);
2) precise platform trajectory (computed by the Institut de Geomatica, Barcelona, using a precise point positioning strategy);
3) platform orientation in the WGS84 reference frame, as measured with the aircraft inertial measurement unit;
4) the vector joining the up-looking and down-looking antenna phase centers in the body frame;
5) antenna phase patterns in the body frame;
6) *a priori* sea state (mss_0) to linearize the forward model, taken from [19].

Fig. 5 shows, for the initial and final epochs when the three GPSs were detected simultaneously, the first pulse-limited footprint (isodelay line 1 C/A code chip away from the specular delay), the antenna footprint (isogain line 3 dB down from the maximum gain), and the glistening zone (iso-σ_o line 3 dB down from the maximum bistatic radar cross section). Clearly, the waveforms from PRN03 must be significantly affected by the antenna pattern. It is also noted that the glistening area is smaller than the pulse-limited footprint.

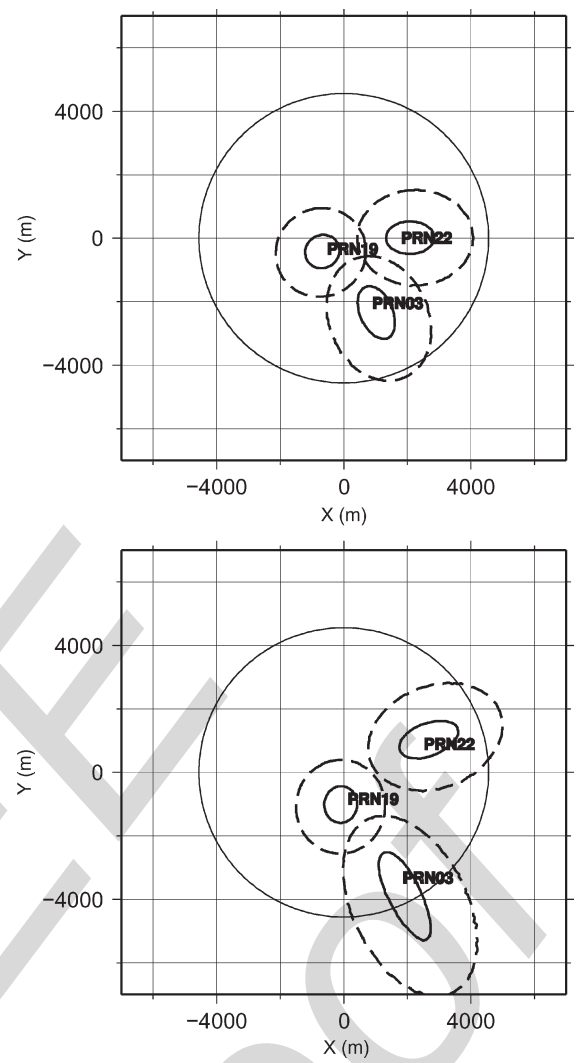

Fig. 5. For the initial and final epochs when the three GPSs were detected simultaneously, we include (discontinuous ellipses) the ISO range corresponding to 300 m for each satellite, (thin circle) the −3-dB gain line corresponding to the down-looking antenna, and (continuous ellipse) the glistening surface defined as the region where the normalized bistatic cross section of the sea surface reduces 3 dB.

TABLE II
MAIN CHARACTERISTICS OF THE REFLECTION EVENTS FOR THE THREE SATELLITES SELECTED: PRN19, PRN22, AND PRN3. THE TYPICAL MSS DURING THE PART OF THE FLIGHT ANALYZED HERE WAS 0.020 (FROM[19]), WHICH WE HAVE USED AS THE A PRIORI VALUE IN OUR MODEL COMPUTATIONS. SODIS FOR SECOND OF THE DAY

PRN	SoD	sin(e)	Az (deg)	$\frac{\partial \tau_{scatt}^{mod}}{\partial mss}(m)$	$\frac{\partial \tau_{spec}^{mod}}{\partial mss}(m)$
19	31749	0.967	237.8	2167	27
19	32649	0.968	210.1	2162	27
19	33649	0.948	185.1	2168	27
22	31749	0.827	89.5	2115	26
22	32649	0.796	78.6	2092	26
22	33649	0.737	68.9	2079	25
3	31749	0.769	156.4	2084	26
3	32550	0.701	154.8	2033	24
3	33649	0.594	153.7	1955	23

Table II summarizes the values of the parameters that are relevant in the description of the reflection events at the beginning, middle, and end of the chosen period.

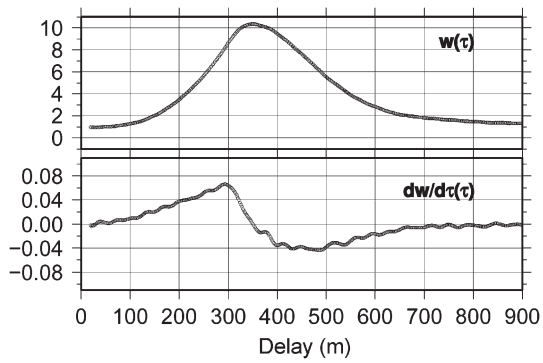

Fig. 6. (Top) Example of a 1-s integrated waveform and (bottom) its derivative collected during the experimental campaign and used in the analysis.

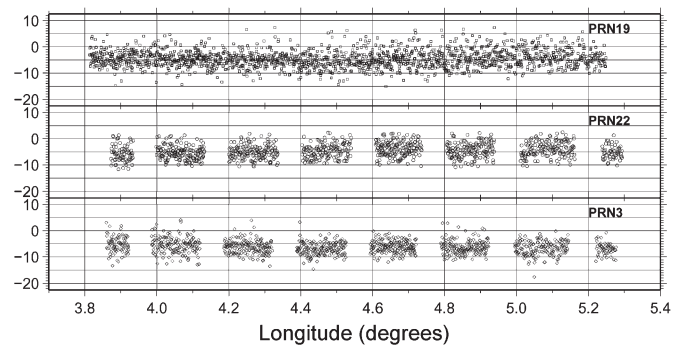

Fig. 7. Altimetric delays $\delta\tau_{\mathrm{spec}}$ (in meters) as a function of the longitude of the corresponding specular point.

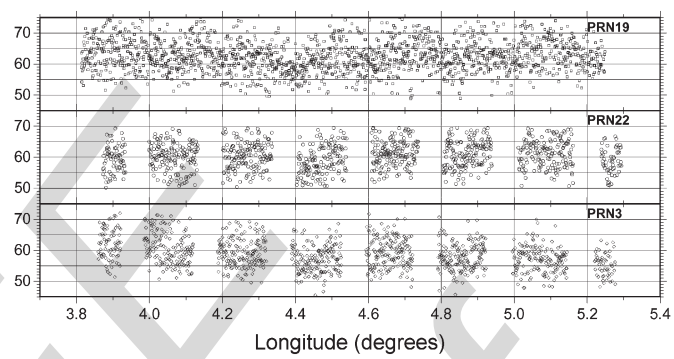

Fig. 8. Scatterometric delays $\delta\tau_{\mathrm{scatt}}$ (in meters) as a function of the longitude of the corresponding specular point.

VII. Data Analysis

The aim of the data analysis is to confirm that the techniques described in this paper perform at the expected uncertainty level, limited in this case by the following: 1) lack of calibration to type-B uncertainties and 2) the use of the C/A code of the GPS signals.

The selected GOLD_RTR data set consisted of $3.8 \times 10^{+6}$ 1-ms complex waveforms. These waveforms were integrated incoherently during 1-s intervals. This produced 1145 1-s integrated waveforms for PRN 3, 1751 for PRN 19, and 1086 for PRN 22. Fig. 6 shows a 1-s integrated waveform and its derivative. As discussed in [7] and [21], an estimate of the expected uncertainty in the measurement σ_τ on the delay is related to the integrated waveforms $w(\tau)$ and its derivative $w'(\tau)$, for high SNR, through the following:

$$\sigma_\tau = \frac{w(\tau)}{w'(\tau)\sqrt{m}}$$

where m is the number of waveforms integrated. After the integration of 1000 1-ms waveforms, we have σ_τ on the order of 4 m.

The delay resolution of the waveforms was 1/20 of a microsecond, or 14.99 m, which was too large compared with σ_τ: The quantization noise was larger than the measurement noise. To solve this issue, we have interpolated the waveforms using Fourier transform algorithms to have an apparent sampling rate that is eight times faster. An alternative procedure using finite impulse response filters has been used in [13] to address a similar problem.

From the integrated waveforms $w(\tau; t, sat)$, and its derivatives $w'(\tau; t, sat)$, we have extracted the quantities $\delta\tau_{\mathrm{spec}}(t, sat)$ and $\delta\tau_{\mathrm{scatt}}(t, sat)$, which are represented in Figs. 7 and 8 as a function of longitude, respectively. Each dot in these figures represents a 1-s delay sample. The number of samples obtained for each PRN is given by N in Table III. Tables III and IV provide the mean, the standard deviation of the 1-s delay samples, and the estimated standard deviation for N-second delay samples. We also include in Fig. 9 the series of the amplitudes of the waveform. The variations of the PRN3 amplitudes are consistent with the changes in the gain shown in Fig. 5. The standard deviation of the 1-s measured altimetric delays is consistent with those obtained in other aircraft experiments [22], [23] and in agreement with the theoretical expectations [7], [24], and the N-sample delay standard deviation of the series, on the order of 10 cm, indicates the potential of the technique to measure the sea-surface height, if the type-B uncertainties are reduced below this quantity.

TABLE III
Computed Mean, Standard Deviation of the 1-s Delay Samples, and the Estimated Standard Deviation for N-Second Delay Samples in the Series of Specular Delays $\delta\tau_{\mathrm{spec}}$ for the Three Satellites PRN19, PRN22, and PRN3. N is the Total Number of 1-s Samples for Each PRN

PRN	mean (m)	1-sec std. dev. (m)	N-sec std. dev. (m)	N
19	-4.55	2.51	0.06	1751
22	-4.58	2.25	0.07	1086
3	-6.21	2.06	0.06	1145

TABLE IV
Computed Mean, Standard Deviation of the1-s Delay Samples, and the Estimated Standard Deviation for N-Second Delay Samples of the Series $\delta\tau_{\mathrm{scatt}}$ for the Three Satellites PRN19, PRN22, and PRN3 (N is Given in Table III)

PRN	mean (m)	1-sec std. dev. (m)	N-sec std. dev. (m)
19	62.49	3.98	0.10
22	60.35	3.58	0.11
3	58.55	3.86	0.11

As shown in Fig. 8 and Table IV, the 1-s standard deviation of the scatterometric delays $\delta\tau_{\mathrm{scatt}}$ is smaller than 4 m. According to the values of the sensitivity of the scatterometric delay with respect to the mss (see the fifth column in Table II), this will represent uncertainties in the mss on the order of 0.002. Such level of uncertainties in the sea-surface roughness will, in turn,

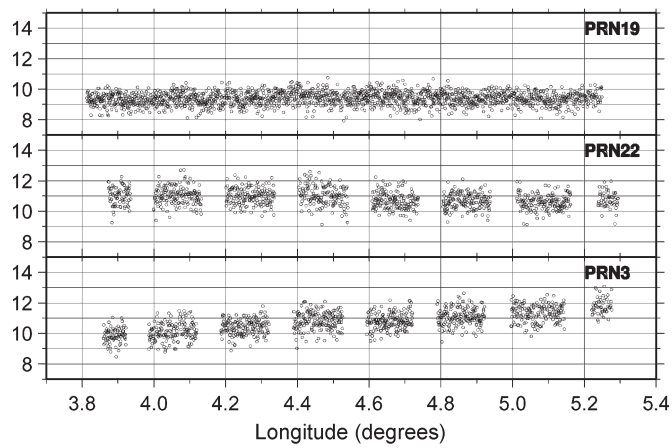

Fig. 9. Amplitude of the waveforms (in arbitrary units) as a function of the longitude of the corresponding specular point.

affect the specular delay (column six in Table II), producing an rms dispersion of 5 cm in $\delta\tau_{\rm spec}$, which is negligible when compared with the 2–3-m standard deviation of the 1-s delays.

As a consequence, we could ignore the contribution of Δmss in (22)

$$\delta\tau_{\rm spec} = -2 \cdot \sin(e) \cdot \Delta h + b_{\rm spec}. \tag{24}$$

In VLBI or GPS, this equation is used to separate the geometrical part from a bias term. Even in the case where the observation uncertainty is very small, a perfect separation is difficult because the range of elevations, as well as other effects like the atmospheric delay, which have similar signatures in the delay, is limited. This is the reason why the VLBI and GPS estimates of vertical components of baselines are less accurate than the horizontal components. Examples of this approach in the analysis of GNSS-R observations for altimetry could be found in [8] and [22]. Separation would therefore require the proper calibration of the instrumental biases, as well as the ingestion of additional relevant information (tropospheric/space weather), as it is done in the RA analysis.

VIII. Discussion

This paper has first formalized the "retracking" of the GNSS reflections by means of the derivative of their waveforms (Sections II and III), which is a method that has the following advantages: 1) being computationally much faster than the standard "retracking" procedure of fitting a model and 2) becoming formally independent of any model. The corresponding algorithms that produce real-time altimetric observables to be used in dedicated digital signal processors have then been presented (Sections IV and V). The overall technique is finally implemented and tested with real data gathered in an airborne experiment (work presented in Sections VI and VII) to check that the uncertainties correspond to the theoretically expected uncertainties and are at the same level with those in similar experiments in which standard "retracking" techniques were used.

The geometry of this particular experiment hindered the separation of some of the type-B uncertainties that typically can be retrieved with GNSS, as it is likely to happen in a hypothetical orbital receiver. Similar problems are faced by RA missions, which successfully solve them by ingestion of external corrections. The results have confirmed that the altimetric performance is not reduced by the technique but limited by the bandwidth of the GNSS signal used (2.026 MHz) and the lack of instrumental calibration. The theoretical range performance improves drastically with a much wider bandwidth instrument (4.5-cm instrument noise and speckle estimated in [25] for a space GNSS-R interferometer), for which the described technique could provide a quick "retracking" method, independent on modeling issues.

Acknowledgment

The authors would like to thank the whole team at the European Space Research and Technology Centre, ESA; Helsinki University of Technology, Espoo, Finland; and TUD who made the CoSMOS-2007 experimental campaigns possible. Some figures were generated using the Generic Mapping Tools version 4 [26].

References

[1] W. Schluter and D. Behrend, "The international VLBI service for geodesy and astrometry (IVS): Current capabilities and future prospects," *J. Geod.*, vol. 81, no. 6–8, pp. 379–387, Jun. 2007.

[2] IGS Central Bureau, M/S 238-540 International GNSS Service Strategic Plan, Pasadena, CA: Jet Propulsion Lab.2009.

[3] V. Rosmorduc, J. Benveniste, O. Lauret, M. Milagro, and N. Picot, Radar Altimetry Tutorial: ESA, CNES2006.

[4] M. Martín-Neira, "A passive reflectometry and interferometry system (PARIS): Application to ocean altimetry," *ESA J.*, vol. 17, no. 4, pp. 331–355, Dec. 1993.

[5] P. Misra and P. Enge, *Global Positioning System: Signals, Measurements, and Performance*. Lincoln, MA: Ganga-Jamuna Press, 2006.

[6] B. N. Taylor and C. E. Kuyatt, *Guidelines for Evaluating and Expressing the Uncertainty of NIST Measurement Results*. Gaithersburg, MD: NIST, 2007.

[7] C. Zuffada and V. Zavorotny, "Coherence time and statistical properties of the GPS signal scattered off the ocean surface and their impact on the accuracy of remote sensing of sea surface topography and winds," in *Proc. IEEE IGARSS*, Aug. 2002, vol. 7, pp. 3332–3334.

[8] G. Ruffini, F. Soulat, M. Caparrini, O. Germain, and M. Martín-Neira, "The Eddy experiment: Accurate GNSS-R ocean altimetry from low altitude aircraft," *Geophys. Res. Lett.*, vol. 31, no. 12, p. L12 306, Jun. 2004.

[9] C. Cox and W. Munk, "Measurement of roughness of the sea surface from photographs of the sun's glitter," *J. Opt. Soc. Amer.*, vol. 44, no. 11, pp. 838–850, Nov. 1954.

[10] L. Amarouche, P. Thibaut, O. Z. Zanife, J.-P. Dumont, Vincent, and N. P. Steunou, "Improving the Jason-1 ground retracking to better account for attitude effects," *Mar. Geod.*, vol. 27, no. 1/2, pp. 171–198, 2004.

[11] S. Maus, C. M. Green, and J. D. Fairhead, "Improved ocean-geoid resolution from retracked ERS-1 satellite altimeter waveforms," *Geophys. J. Int.*, vol. 134, no. 1, pp. 243–253, Jul. 1998.

[12] V. U. Zavorotny and A. G. Voronovich, "Scattering of GPS signals from the ocean with wind remote sensing application," *IEEE Trans. Geosci. Remote Sens.*, vol. 38, no. 2, pp. 951–964, Mar. 2000.

[13] S. T. Lowe, C. Zuffada, Y. Chao, P. Kroger, L. E. Young, and J. L. LaBrecque, "5-cm precision aircraft ocean altimetry using GPS reflections," *Geophys. Res. Lett.*, vol. 29, no. 10, p. 1375, May 2002.

[14] E. Cardellach, G. Ruffini, D. Pino, A. Rius, A. Komjathy, and J. L. Garrison, "Mediterranean balloon experiment: Ocean wind speed sensing from the stratosphere, using GPS reflections," *Remote Sens. Environ.*, vol. 88, no. 3, pp. 351–362, 2003.

[15] G. A. Hajj and C. Zuffada, "Theoretical description of a bistatic system for ocean altimetry using the GPS signal," *Radio Sci.*, vol. 38, no. 5, pp. 1–10, Oct. 2003.

[16] J. L. Garrison, A. Komjathy, V. U. Zavorotny, and S. J. Katzberg, "Wind speed measurement using forward scattered GPS signals," *IEEE Trans. Geosci. Remote Sens.*, vol. 40, no. 1, pp. 50–65, Jan. 2002.

[17] R. Bracewell, *The Fourier Transform and Its Applications*. New York: McGraw-Hill, 1965.

[18] O. Nogués-Correig, E. Cardellach Gali, J. Sanz Campderros, and A. Rius, "A GPS-reflections receiver that computes Doppler/delay maps in real time," *IEEE Trans. Geosci. Remote Sens.*, vol. 45, no. 1, pp. 156–174, Jan. 2007.

[19] E. Cardellach and A. Rius, "A new technique to sense non-Gaussian features of the sea surface from L-band bi-static GNSS reflections," *Remote Sens. Environ.*, vol. 112, no. 6, pp. 2927–2937, Jun. 2008.

[20] F. G. Lemoine, S. C. Kenyon, J. K. Factor, R. G. Trimmer, N. K. Pavlis, D. S. Chinn, C. M. Cox, S. M. Klosko, S. B. Luthcke, M. H. Torrence, Y. M. Wang, R. G. Williamson, E. C. Pavlis, R. H. Rapp, and T. R. Olson, "The development of the joint NASA GSFC and the NIMA geopotential model EGM96," NASA, Washington, DC, Tech. Rep. TP-1998-206861, Jul. 1998.

[21] S. D'Addio, C. Buck, and M. Martin-Neira, "PARIS altimetry precision with Galileo signals-in-space," in *Proc. IEEE IGARSS*, Jul. 2008, vol. 3, pp. III-63–III-65.

[22] A. Rius, J. M. Aparicio, E. Cardellach, M. Martín-Neira, and B. Chapron, "Sea surface state measured using GPS reflected signals," *Geophys. Res. Lett.*, vol. 29, no. 23, p. 2122, Dec. 2002.

[23] G. Ruffini, F. Soulat, M. Caparrini, O. Germain, and M. Martín-Neira, "The Eddy experiment (09252002): Mesoscale altimetry using GPS-R (L1-C/A) from low altitude aircraft," in *Proc. Workshop Oceanogr. GNSS Reflections*, Jul. 17–18, 2003, pp. 31–38.

[24] S. J. Katzberg, J. L. Garrison, and C. T. Howell, "Simple over-water altimeter using GPS reflections," in *Proc. 12th Int. Tech. Meeting Satell. Division Inst. Navig. ION GPS*, Sep. 1999, pp. 1819–1827.

[25] ESA D/TEC-ETP, Dossier Paris In-Orbit Demonstrator, Feb. 2009.

[26] P. Wessel and W. H. F. Smith, "New, improved version of generic mapping tools released," *EOS, Trans. Amer. Geophys. Union*, vol. 79, no. 47, p. 579, 1998.

Antonio Rius received the Ph.D. degree in astrophysics from Barcelona University, Barcelona, Spain, in 1974.

From 1975 to 1985, he was a Member of the Technical Staff with the Deep Space Communications Complex, National Aeronautics and Space Administration, Madrid, Spain, where he was responsible for the radio astronomical activities. Since 1986, he has been with the Institut de Ciè(c)ncies de l'Espai, Consejo Superior de Investigaciones Cientèficas, Institut d'Estudis Espacials de Catalunya, Bellaterra, Spain, where he is currently responsible for the Earth Observation Research Group. His current research interests include applications to Earth Science of Global Navigation Satellite Systems.

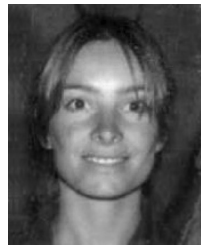

Estel Cardellach received the B.S. degree physics from the Autonomous University of Barcelona, Barcelona, Spain, in 1997 and the Ph.D. degree from the Department of Signal Theory and Communications, Polytechnic University of Catalonia, Barcelona, in 2002.

She has been working on scientific applications of Global Navigation Satellite Systems for remote sensing of the Earth, mostly focused on assessing the geophysical information content of the GPS signals reflected off by oceans. She was a Postdoctoral Researcher with the Harvard Smithsonian Center for Astrophysics, Cambridge, MA (in 2003–2005). She is currently with the Institut de Ciè(c)ncies de l'Espai, Consejo Superior de Investigaciones Cientèficas, Institut d'Estudis Espacials de Catalunya (IEEC), Bellaterra, Spain, under a Ramón y Cajal contract.

Dr. Cardellach was a National Research Council Awardee for a postdoctoral position at the National Aeronautics and Space Administration/Jet Propulsion Laboratory, Pasadena, CA (in 2002–2003) and a Spanish Ministry for Education and Science Program Juan de la Cierva Awardee (in 2005–2008) at IEEC, Barcelona.

Manuel Martín-Neira (M'96–SM'07) received the M.S. and Ph.D. degrees in telecommunication engineering from the School of Telecommunication Engineering, Polytechnic University of Catalonia, Barcelona, Spain, in 1986 and 1996, respectively.

From 1989 to 1992, he was with GMV, which is a Spanish firm, where he was responsible for several projects for the European Space Agency (ESA) related to GPS spacecraft navigation with applications to precise landing and attitude determination. Since 1992, he has been with the European Space Research and Technology Centre, ESA, Noordwijk, The Netherlands, where he is in charge of the radiometer activities within the Payload, Equipment and Technology Section and is currently an Instrument Principal Engineer of ESA's Soil Moisture and Ocean Salinity Earth Explorer Opportunity Mission. During this period, he has also developed new concepts for constellations of small satellites for Earth observation. In particular, he holds a patent on the Passive Reflectometry and Interferometry System concept for the use of Global Navigation Satellite System signals reflected from the ocean.

Dr. Martín-Neira was the recipient of a fellowship to work on radiometry at the European Space Research and Technology Center, Noordwijk, in 1988 and the Confirmed Inventor Award from the director of ESA in 2002. He has been a member of the Academie des Technologies of France since 2009.

AUTHOR QUERIES

AUTHOR PLEASE ANSWER ALL QUERIES

AQ1 = "ESP2007-30996-E," "AYA2008-05906-C02-02," and "ECN 20069/06/NL/EL" were captured as grant numbers. Please check if appropriate.
AQ2 = "European Space Agency" was taken as the expanded form of the acronym "ESA." Please check if appropriate.
AQ3 = The first part of the acknowledgment was captured in the first footnote. Please check.
AQ4 = "CSIC" and "IEEC" were defined as "Consejo Superior de Investigaciones Cientèficas" and "Institut d'Estudis Espacials de Catalunya," respectively. Please check if correct. Moreover, "Intitut de Ciències del Espai" was changed to "Institut de Ciències de l'Espai." Please check if appropriate.
AQ5 = Please validate the address and postal code provided for "Institut de Ciéncies de l'Espai, Consejo Superior de Investigaciones Cientèficas, Institut d'Estudis Espacials de Catalunya."
AQ6 = "ESTEC" was defined as "European Space Research and Technology Centre." Please check if correct.
AQ7 = Please validate the address and postal code provided for "European Space Research and Technology Centre, European Space Agency."
AQ8 = In the following list, "uncertainties type A" and "uncertainties type B" were changed to "type-A uncertainties" and "type-B uncertainties." Please check if OK.
AQ9 = "Direct" was changed to "direct signal."
AQ10 = "PRN" was defined as "pseudorandom noise." Please check if correct.
AQ11 = "C/A" was defined as "coarse/acquisition." Please check if correct.
AQ12 = "Coarse, C/A, code" was changed to "C/A code" (C/A was already defined as "coarse/acquisition"). Please check if OK.
AQ13 = The sentence was reworded. Please check if the intended meaning was retained.
AQ14 = Please check the changes made in the sentence if the intended meaning was retained.
AQ15 = "TKK" was defined as "Helsinki University of Technology." Please check if appropriate.
AQ16 = Please provide the expanded form of the acronym "TUD."
AQ17 = "NASA" was defined as "National Aeronautics and Space Administration." Please check if correct.
AQ18 = "Postdoc" was changed to "Postdoctoral Researcher." Please check if appropriate.
AQ19 = The author's current affiliation was changed to "Institut de Cincies de l'Espai, Consejo Superior de Investigaciones Cientèficas, Institut d'Estudis Espacials de Catalunya" for consistency. Please check if appropriate.
AQ20 = The author's current affiliation was changed to "European Space Research and Technology Centre, ESA, Noordwijk, The Netherlands" for consistency with the one in the footnote. Please check if appropriate.

END OF ALL QUERIES